ELSEVIER

Journal of Chromatography A, 928 (2001) 13–23

JOURNAL OF CHROMATOGRAPHY A

www.elsevier.com/locate/chroma

Characterization and modeling of monolithic stationary phases: application to preparative chromatography

Sanchayita Ghose[1], Steven M. Cramer*

Department of Chemical Engineering, Rensselaer Polytechnic Institute, Troy, NY 12180, USA

Received 3 January 2001; received in revised form 5 July 2001; accepted 11 July 2001

Abstract

A methodology for characterizing and modeling preparative separations on monolithic ion-exchange stationary phases is presented. A dimensionless group analysis was carried out to determine the relative importance of mass transfer and kinetic resistances on this stationary phase. In contrast to conventional beaded morphologies, the continuous bed stationary phase was found to possess enhanced mass transport properties resulting in kinetic resistance as the dominant non-ideality. Accordingly, a reaction-dispersive steric-mass action formalism was successfully utilized for simulating preparative displacement chromatography on this resin. Since kinetics were found to be important on this column morphology, mobile phase salt concentration was found to be an important variable during displacement chromatography on this stationary phase. An increase in the mobile phase salt concentration was found to significantly improve the displacement separation of a model protein mixture. The formalism presented in this paper provides a better understanding of preparative chromatography in monolithic resin systems and a means of simulating separations on this class of chromatographic stationary phases.

Keywords: Monolithic stationary phases; Steric mass action; Mass transport models; Stationary phases, LC; Ion exchange

1. Introduction

Chromatography is the most widely employed preparative purification tool in the biotechnology industry. It has been well documented that the rate of mass transport of biomolecules to the interior binding sites is typically the dominant contribution to band broadening in chromatographic systems [1]. The last decade has seen a plethora of chromatographic stationary phase materials based on new concepts to increase speed at both analytical and preparative scale. Some of these novel stationary phase materials include perfusive [2], gel in a shell [3], super porous [4], and membrane-based systems [5].

Continuous bed chromatographic columns (a.k.a. monolithic stationary phases) are another novel concept aimed at accelerating mass transport to minimize band broadening which in turn can result in high column efficiency and better performance at elevated flow-rates [6].

Hjerten patented the technology of ''continuous bed chromatography'' at the University of Uppsala in Sweden [7]. The continuous bed matrix is comprised of a polymeric monolith that is formed in the chromatographic column tube. Svec and coworkers

*Corresponding author.

E-mail address: crames@rpi.edu (S.M. Cramer).

[1]Currently at Immunex Corporation, Seattle, WA.

0021-9673/01/$ – see front matter
PII: S0021-9673(01)01115-3

have developed novel continuous macroporous rod separation media and used it successfully for high speed separation of proteins and polypeptides in reversed-phase, ion-exchange, hydrophobic interaction and affinity modes [8]. They have also demonstrated the separation of oligonucleotides on these ''molded'' monolithic rods with ion-exchange functional surfaces [9]. Minakuchi et al. [10] have shown the performance of an octadecylsilated continuous porous silica column in polypeptide separations. Gustavsson et al. [11] have described the preparation and use of superporous agarose continuous beds for chromatography and electrophoresis. Garke et al. [12] have used an UNO S1 (BioRad, Hercules, CA) column for analysis and purification of rh-bFGH. Freitag and Giovannini [13] have shown chromatographic separation of supercoiled plasmid DNA on these systems and compared it to high-performance membrane chromatography. Freitag and Vogt [14] have demonstrated displacement separations of α-lactalbumin and β-lactoglobulin using an UNO anion-exchange stationary phase. In addition, these authors have also shown displacement separations of plasmid DNA from protein and bacterial lipopolysaccharides on this resin [15]. The performance of particulate and continuous bed columns for protein displacement chromatography have also been compared [16].

To date, there has not been much work reported in the literature on the modeling of chromatographic separations on monolithic stationary phases. Liapis and Meyers [17] have determined the values of the intraparticle interstitial velocity and the pore diffusivity of the adsorbate by a cubic lattice network model. However, no comprehensive study has been carried out to compare the relative effects of mass transport and kinetics and to model preparative protein purification on this stationary phase material.

In this manuscript, mass transport and kinetics are characterized on an UNO monolithic stationary phase material. Three model proteins are employed to illustrate the resin characterization methodology. Pulse injections under retained and unretained conditions are employed to estimate the transport and kinetic parameters for these proteins. Dimensionless groups are then constructed to evaluate the relative contributions of the various transport mechanisms. This analysis is then used to determine the most appropriate rate model for this resin material. Finally, this model is employed in concert with the Steric Mass Action (SMA) isotherm to model preparative protein separations on continuous bed columns.

2. Theory

2.1. Adsorption model

The SMA formalism [18] is a three-parameter model for the description of multicomponent protein–salt equilibrium in ion-exchange systems. The multipointed binding of the protein molecule to the stationary phase is represented as a stoichiometric exchange of mobile phase protein and bound counter ions. The model thus involves three parameters for each solute: the characteristic charge (ν) which is the average number of sites that a molecule interacts with on the surface; the steric factor (σ) which is the average number of sites on the surface which are sterically shielded by the macromolecule and the equilibrium constant (K) of the exchange reaction between the solute and the salt counter-ions on the surface.

The equation for the SMA isotherm for a single component is given as:

$$K = \left(\frac{Q}{C}\right)\left(\frac{C_{\text{salt}}}{\Lambda - (\nu + \sigma)Q}\right)^{\nu} \quad (1)$$

where Q and C are the solute concentrations on the stationary and mobile phases, respectively and C_{salt} is the mobile phase salt concentration. The SMA isotherm is an implicit isotherm that can successfully predict non-linear, multicomponent behavior over a range of mobile phase salt concentrations once the parameters (K, ν and σ) have been determined. This thermodynamic model has been shown to accurately predict ion-exchange chromatographic behavior in isocratic [19], gradient [20] and displacement chromatography [21].

2.2. Transport model

The most complete transport model that can describe the chromatographic behavior of solutes is the general rate model [22]. However, since it is

computationally very expensive, it is often desirable to employ lumped rate models such as the transport-dispersive and reaction-dispersive models. The lumped models are as described below:

2.2.1. Transport dispersive model

This model employs a solid film linear driving force approximation:

$$\frac{\partial C_i}{\partial \tau} + \beta \frac{\partial Q_i}{\partial \tau} + \frac{\partial C_i}{\partial x} = \frac{1}{Pe_a} \frac{\partial^2 C_i}{\partial x^2} \tag{2}$$

$$\frac{\partial Q_i}{\partial \tau} = St_i(Q_i^{equil} - Q) \tag{3}$$

The symbols are defined in the Nomenclature section. In this model, the Peclet number, Pe_a, accounts for axial dispersion effects whereas the Stanton number, *St*, represents a lumped mass transport coefficient that accounts for film, pore and/or surface diffusion effects (depending on the relative importance of these phenomena).

2.2.2. Reaction-dispersive model

$$\frac{\partial C_i}{\partial \tau} + \beta \frac{\partial Q_i}{\partial \tau} + \frac{\partial C_i}{\partial x} = \frac{1}{Pe_a} \frac{\partial^2 C_i}{\partial x^2} \tag{4}$$

$$\frac{\partial Q_i}{\partial \tau} = k_{ads} C_i \bar{Q}_1^{\nu} - k_{des} C_{salt}^{\nu} Q_i \tag{5}$$

Eq. (5) has been written for the SMA formalism as this isotherm model can be represented as a stoichiometric exchange of mobile phase protein and bound counter ions. This rate model can be employed when the kinetics of adsorption–desorption is the rate limiting resistance.

Rearrangement of terms in Eq. (5) yield the following result:

$$\frac{\partial Q_i}{\partial t} = k_{des} C_{salt}^{\gamma} \left(\frac{k_{ads} C_i \bar{Q}_1^{\gamma}}{k_{des} C_{salt}^{\gamma}} - Q_i \right) \tag{6}$$

$$\Rightarrow \frac{\partial Q_i}{\partial t} = k_{des} C_{salt}^{\gamma} (Q_{i\,equil} - Q_i) \tag{7}$$

Thus the reaction dispersive model can also be written in an analogous form to the solid film linear driving force model (Eq. (3)).

Finite difference techniques have been employed to solve the mass transport equations in both of these models. Since the SMA isotherm is implicit, a Newton–Raphson technique was employed for the equilibrium calculations in this paper. The temporal terms were discretized using forward differences while the convection and diffusion terms were discretized using backward and central differences, respectively [23]. The discretized equations were solved subject to the following stability criteria:

$$\frac{\Delta \tau}{Pe_i (\Delta x)^2} < 0.2 \tag{8}$$

$$\frac{\Delta \tau}{\Delta x} < 1 \tag{9}$$

2.3. Estimation of transport parameters

In this work, the dependence of HETP on two operational parameters (flow-rate and salt concentration) has been analyzed to estimate the appropriate rate parameters for protein separations in ion-exchange systems [24]. These factors account for the non-ideality of the system and contribute to increasing the HETP of the system. The general rate model in conjunction with the Steric Mass Action formalism under linear adsorption conditions was transformed into the Laplace domain. Subsequently, the HETP equations were derived using the first and second moments of the solution in the Laplace domain. The following equations relate the effect of flow-rate and the salt concentration on the HETP of protein pulses in ion-exchange systems [24]:

$$H = \frac{2D_a}{u} + \frac{2(1-\varepsilon_i)\varepsilon_p b_o^2 u}{[\varepsilon_i + (1-\varepsilon_i)\varepsilon_p b_o]^2} \times \left[\frac{R}{3k_f} + \frac{R^2}{15D_p(1+[b_o-1]r)} + \frac{(b_o-1)^2}{b_o^2 k''_{des}} \right] \tag{10}$$

The various symbols are defined in the Nomenclature section. The operational parameters are u (the linear velocity) and b_o, which is related to the retention factor k' ($b_o = 1 + k'$). As can be seen in the above equations, there are five rate parameters to be estimated: the axial dispersion parameter, D_a, the film mass transfer coefficient, k_f, the pore diffusion

coefficient, D_p, the surface diffusion coefficient, D_s and the desorption rate constant, k_{des}.

Now, the axial dispersion parameter, D_a, can be divided into contributions from molecular diffusion and eddy diffusion. For macromolecular systems, the contributions from molecular diffusion are usually negligible [24]. Hence the axial dispersion parameter can be defined as follows:

$$D_a = \zeta u \tag{11}$$

where ζ is a proportionality factor. Thus, Eq. (10) becomes

$$H = 2\zeta + \frac{2(1-\varepsilon_i)\varepsilon_p b_o^2 u}{[\varepsilon_i + (1-\varepsilon_i)\varepsilon_p b_o]^2} \times \left[\frac{R}{3k_f} + \frac{R^2}{15D_p(1+[b_o-1]r)} + \frac{(b_o-1)^2}{b_o^2 k''_{des}} \right] \tag{12}$$

For the estimation of these parameters, pulse techniques under retained and unretained conditions were employed. From Eq. (12), it can be seen that the contributions to the HETP from the mass transfer and the kinetic resistance are additive. Thus, operating under unretained conditions suppresses the contributions from surface diffusion and adsorption/desorption kinetics. In other words, under unretained conditions, $b_o = 1$ and hence:

$$H = 2\zeta + \frac{2(1-\varepsilon_i)\varepsilon_p u}{[\varepsilon_i + (1-\varepsilon_i)\varepsilon_p]^2} \left[\frac{R}{3k_f} + \frac{R^2}{15D_p} \right] \tag{13}$$

The film mass transfer coefficient, k_f, is estimated from well-established correlation [24].

Once k_f has been determined, the other two parameters D_p and ζ in Eq. (13) were fitted using the HETP vs. u data under unretained conditions. HETPs were then determined under retained conditions at various combinations of salt concentration (corresponding to different values of b_o) and linear velocity u. This data was then used to fit the remaining two parameters D_s and k_{des} in Eq. (12).

3. Experimental methods

3.1. Materials

Sodium monobasic phosphate, sodium dibasic phosphate, sodium nitrate, α-chymotrypsinogenA, ribonucleaseA, horse cytochromeC, neomycin sulfate (displacer) and blue dextran were purchased from Sigma Chemical (St. Louis, MO). Sodium chloride was purchased from Aldrich Chemical (Milwaukee, WI). The UNO-S6 column (12×53 mm) with strong cation-exchange sulfopropyl functional group was donated by BioRad (Hercules, CA). The G2000SW$_{XL}$ SEC column (0.78 cm (D)×30 cm (L)) was obtained from TosoHaas (Montgomeryville, PA).

3.2. Apparatus

Pulse injections and protein analysis were made using a WISP model 712 autoinjector (Waters Corporation, Milford, MA) connected to a model 650E Advanced Protein Purification system (Waters Corporation, Milford, MA) with a model 484 Tunable Absorbance Detector (Waters Corporation, Milford, MA). Data acquisition and processing were carried out using a Millennium 2010 chromatography workstation (Waters Corporation, Milford, MA). Sodium nitrate was monitored at 310 nm while the proteins were monitored at 254 nm.

All displacement experiments were carried out using a Model 590 programmable HPLC pump (Waters, Milford, MA) connected to the chromatographic columns via a Model C10W 10-port valve (Valco, Houston, TX, USA). All gradient experiments were carried out using a Waters 600 Multisolvent Delivery System (Waters, Milford, MA) connected to the chromatographic columns via a Model C10W 10-port valve (Valco, Houston, TX, USA). Fractions of the column effluent were collected using LKB 2212 Helirac fraction collector (LKB, Sweden).

3.3. Estimation of SMA parameters of proteins

The linear SMA parameters of the proteins (K and ν) were determined using the protocols outlined by Gadam et al. [25]. Briefly, the characteristic charge and the equilibrium constant were determined using linear elution retention data at different mobile phase salt concentrations. The nonlinear parameter (σ, steric factor) was obtained from frontal experiments carried out at a single salt concentration (typically, $<$100 mM) at low flow-rates.

3.4. Estimation of SMA parameters of displacer

The characteristic charge of the displacer was determined from the induced salt gradient produced from passing a front. The characteristic charge is given by the ratio of the magnitudes of the induced salt gradient to the displacer concentration. The equilibrium constant and the steric factor were then determined by a best fit of the adsorption isotherms of the displacer obtained at various mobile phase salt concentrations [18].

3.5. Estimation of transport parameters of proteins and the displacer

Pulse injections of the proteins were made to determine the transport parameters (as described in Section 2.3). HETPs were calculated by fitting Gaussian curves to the peaks obtained from pulse injections. HETP of the fitted Gaussian peaks were calculated using the following equation:

$$H = \frac{L}{5.54}\left(\frac{t_{w,0.5}}{t_r}\right)^2 \quad (14)$$

Using a Gaussian fit helps eliminate errors in the second moment calculations due to instrument noise.

The lumped transport parameter for the displacer was obtained by a least square fit of the breakthrough curves of the displacers at two different flow-rates [23].

3.6. Displacement experiments

The column was initially equilibrated with the carrier and then subsequently perfused with feed, displacer and regenerant solutions. The feed load, salt concentration and displacer concentration employed for the separation are given in the figure legends of the respective chromatograms. Fractions of the column effluent were collected for subsequent analysis of protein and displacer concentration in the effluent. Experimental details for each separation are listed in the figure legends.

3.7. Protein analysis

Fractions for α-chymotrypsinogenA/horse cytochromeC separations were analyzed by size exclusion HPLC under isocratic conditions. A mobile phase of 50 m*M* sodium phosphate, pH 6, containing 150 m*M* sodium chloride was employed. The column effluent was monitored at 254 nm by an UV–Vis detector.

3.8. Displacer analysis

Neomycin sulphate was analyzed using a phenol–sulfuric acid assay [26]. The fractions were diluted to be within the linear range of the assay (0.01–0.1 m*M*). 0.8 ml of the sample was mixed with 3.2 ml of sulfuric acid, reacted for 1 min, and cooled to room temperature. 50 μl of 90% phenol (w/v) was then added and the resultant mixture allowed to equilibrate for 30 min. The absorbance was read at 480 nm.

4. Results and discussion

4.1. Morphology of the column bed

UNO continuous bed columns are prepared by a process of in-column polymerization of acrylic acid and *N*,*N*′-methylenebisacrylamide [6]. In contrast to conventional particulate media, these columns are composed of a single, monolithic polymer rod. In order to use the HETP equations (Eqs. (10)–(13)) it is necessary to estimate an effective particle diameter for the column. This was carried out by measuring the pressure drop across the column as a function of linear velocity. Fig. 1 shows pressure drop versus linear velocity data on an UNO S6 column using water as the mobile phase. The particle diameter was approximated by using the Kozeny–Carman equation [27] which gave an effective value of 3 μm. This

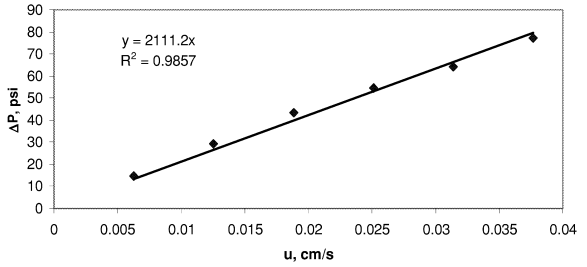

Fig. 1. Pressure drop vs. linear velocity plot to find the equivalent particle diameter (column porosity = 0.8).

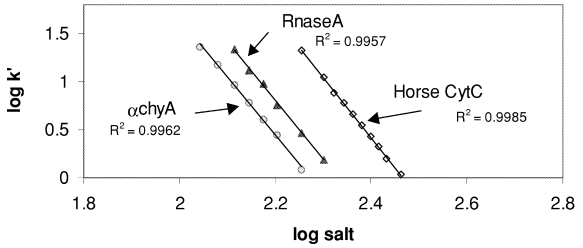

Fig. 2. Log k' vs. log (salt concentration) plot for the three proteins – (α chymotrypsinogenA, ribonucleaseA, horse cytochromeC).

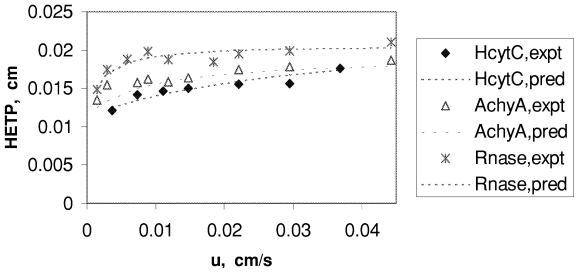

Fig. 3. HETP plots for the three proteins under unretained conditions. Mobile phase: 1 *M* NaCl in 50 m*M* phosphate buffer (pH 6). Dashed lines are least squares fits to the data points.

value is in agreement with the SEM photographs of UNO stationary phase by Garke et al. [12]. In this paper, the authors indicate the presence of particle like structures with diameters ranging from 2 to 3 μm which are interconnected thereby forming a network of open channels. The presence of these open channels and the high porosity of the bed ensure a low pressure drop across the column. Moreover Bidlingmaier et al. [28] have also fitted the Van Deemter parameters for a monolithic C_{18} bonded reversed-phase column by assuming a particle diameter of 5 μm and showed that it has similar performance to microparticulate 5-μm C_{18} bonded columns.

4.2. Thermodynamic parameters of the proteins

Fig. 2 shows the linear log k'–log salt plots for the three proteins α-chymotrypsinogenA, ribonucleaseA, horse cytochromeC. This plot is used to determine the linear SMA parameters (K and ν). In addition, frontal experiments were carried out to determine the non-linear parameter σ. The SMA parameters for the three proteins are listed in Table 1.

4.3. Estimation of transport parameters and dimensionless group analysis

Fig. 3 illustrates the variation of the HETP of the proteins as a function of the linear velocity under unretained conditions. As seen in the figure, under these conditions the HETPs are relatively independent of the flow-rate. This behavior is commonly observed for perfusive chromatographic systems, which have been shown to exhibit convective-augmented diffusion [2]. In these systems, the corrected pore diffusivity (D') of solutes have generally been found by using the functional form of Rodrigues et al. [29] for spherical particles as given by:

$$D_p = \frac{D'}{f(\lambda_p)} \tag{15}$$

where

$$f(\lambda_p) = \frac{3}{\lambda_p}\left(\frac{1}{\tanh \lambda_p} - \frac{1}{\lambda_p}\right) \tag{16}$$

$$\lambda_p = \frac{u'R}{3D_p} \tag{17}$$

Table 1
SMA parameters for the three proteins (Λ = 750 m*M*/volume of stationary phase; β = 0.28)

Protein	ν	K	σ
α-ChymotrypsinogenA	5.43±0.1	2.92 e−3±0.3e−3	153±30
RibonucleaseA	5.69±0.18	3.35 e−3±0.35e−3	118±22
Horse cytochromeC	6.08±0.1	12.39 e−3±1e−3	125±25

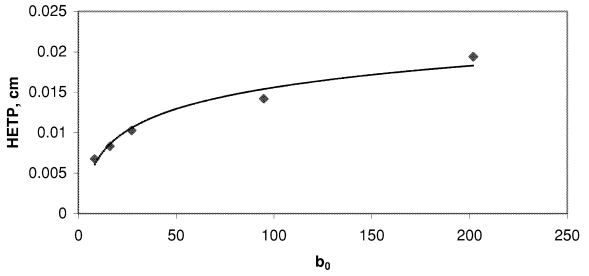

Fig. 4. Variation of HETP as a function of b_o for α-chymotrypsinogenA. Solid lines are least squares fits to the data points.

The various symbols above are defined in the Nomenclature section.

A first order approximation of Eq. (16) was used in conjunction with Eq. (13) to fit the HETP vs. linear velocity, u data. Fig. 3 shows a comparison of the predicted and experimental HETP vs. u plots. As can be seen in the figure, the functional form for convectively augmented diffusive systems can adequately describe the behavior of the continuous bed chromatographic system. Fitting the HETP vs. u data under unretained conditions enabled the determination of the mass transport parameters D_p and ζ.

HETP values were then determined under retained conditions at a variety of salt concentrations and flow-rates. A representative plot of the HETP versus b_o (which is a function of salt concentration) is shown in Fig. 4. Since this curve is monotonically increasing it is indicative of a chromatographic system with negligible surface diffusion (i.e. $D_s = 0$) [24]. A least square fit of the HETP vs. u data under retained conditions enabled an estimation of the desorption rate constant (k_{des}). Fig. 4 shows an overlay of experimental and fitted values of HETP vs. b_o for α-chymotrypsinogenA.

Table 3
Dimensionless groups employed in this manuscript

Dimensionless groups	Description
$N_p = \frac{D_p L}{R^2 u}$	$\frac{\text{Pore diffusion}}{\text{Convection}}$
$N_s = \left(\frac{1-\varepsilon_p}{\varepsilon_p}\right)\frac{D_s L}{R^2 u} K_{SMA}\left(\frac{\bar{Q}_1}{C_{salt}}\right)^{\nu}$	$\frac{\text{Surface diffusion}}{\text{Convection}}$
$N_{des} = \frac{k_{des} C_{salt}^{\nu} L}{u}$	$\frac{\text{Desorption kinetics}}{\text{Convection}}$
$N_f = \frac{3 k_f L}{R u}$	$\frac{\text{Film transport}}{\text{Convection}}$
$\frac{1}{N_{Pe}} = \frac{D_a}{L u}$	$\frac{\text{Axial dispersion}}{\text{Convection}}$

Using the transport and kinetic parameters (listed in Table 2) determined above, several dimensionless groups were determined to ascertain the relative importance of the various transport mechanisms [24]. Table 3 lists the dimensionless groups employed in this study and Table 4 presents their values for the various proteins. The dimensionless groups relate the rates of the various transport mechanisms to the convective transport rate. The lowest value of the dimensionless group gives the dominant non-ideality of the system. From the values of the dimensionless groups, it can be seen that the adsorption/desorption process in the rate limiting step for this system. Accordingly, the reaction-dispersive model was selected for simulating preparative separations on this stationary phase.

Table 2
Transport parameters for the three proteins

	α-ChymotrypsinogenA	RibonucleaseA	Horse cytochromeC
D_p	7.44e−10 (1+119u)	1.15e−10 (1+590u)	2.8e−9 (1+32.11u)
D_a	0.03u	0.027u	0.03u
k_f	6.14e−4	7.23e−4	7.56e−4
D_s	–	–	–
k_{des}	4.92e−12	4.52e−12	40.4e−12

Table 4
Dimensionless groups for the three proteins

	α-ChymotrypsinogenA	RibonucleaseA	Horse cytochromeC
N_p	20.83 + 0.175/u	15.93 + 0.027/u	31.15 + 0.659/u
N_{Pe}	938	1038	938
N_f	65.1/u	76.6/u	80.1/u
N_s	No surface diffusion	No surface diffusion	No surface diffusion
N_{des}	0.0438/u	0.11/u	4.511/u

4.4. Modeling of preparative protein purification

The reactive-dispersive SMA model (Eqs. (4)–(7)) was employed to predict the performance of displacement separations and to investigate the effect of various operating conditions. Displacement experiments with two of the model proteins α-chymotrypsinogenA and horse cytochromeC were carried out to investigate the effect of mobile phase salt concentration on this separation. The specific experimental conditions are mentioned in the figure legends of the respective chromatograms. As seen in Fig. 5a and b, a dramatic improvement in performance was observed when the salt concentration was increased from 50 to 80 m*M*. It is to be expected that an increase in the salt concentration would help to improve the desorption kinetics of the system and thereby facilitate displacement separations. Thus, these results provide further evidence that the kinetics of the adsorption–desorption process plays an important role in the performance of this monolithic material. The model predictions are also presented in these figures. Clearly, the reactive-dispersive SMA model is able to capture this strong dependence on salt concentration.

This strong dependence on background salt concentration is significant in that the selection of an appropriate salt concentration is regarded as a secondary variable during displacement chromatography. Generally, a low background salt concentration is selected to enhance capacities during displacement separations. However, as was seen in Fig. 5a and b, buffer salt concentration had a significant impact on the displacement separation. Clearly, buffer (and load sample) salt concentration can be significant in displacement separations, particularly when kinetics is the dominant non-ideality on a chromatographic stationary phase.

4.5. Significance of selecting an appropriate model

As seen above, the reactive-dispersive model is well equipped to describe displacement separations in these monolithic materials. The obvious question then arises, is there anything unique about this model and could another transport model also capture the behavior of this system? In order to investigate this, the simulations were also carried out using the

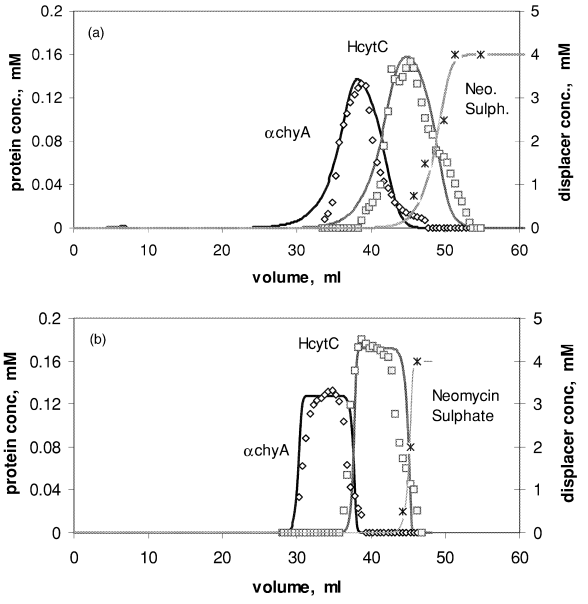

Fig. 5. Comparison of experimental and simulation results for the displacement separation of α-chymotrypsinogenA and horse cytochromeC. Solid lines are simulation results from the reaction-dispersive model. Feed load: 2.5 ml of 0.5 m*M* horse cytochromeC and 0.382 m*M* α-chymotrypsinogenA. Fraction size: 500 μl; Displacer: 4 m*M* neomycin sulfate. (a) Mobile phase: 50 m*M* phosphate buffer (pH 6), flow-rate: 0.5 ml/min; (b) Mobile phase: 50 m*M* phosphate buffer (pH 6) in 80 m*M* Na^+, flow-rate: 0.5 ml/min.

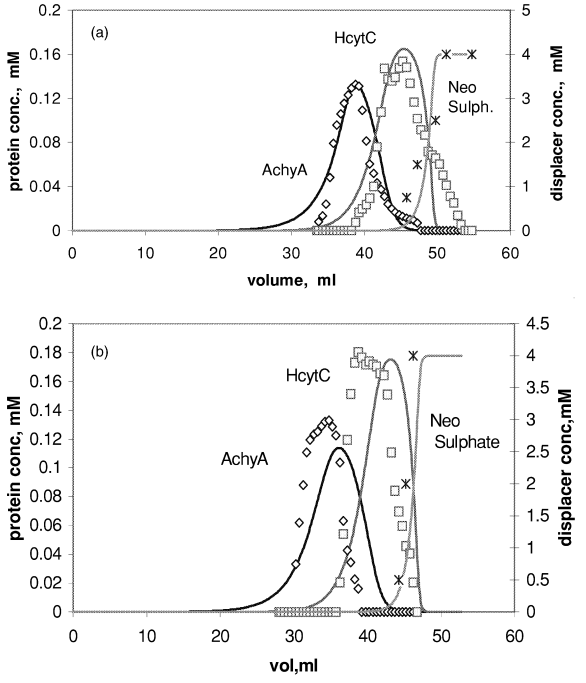

Fig. 6. Comparison of experimental and simulation results from the transport-dispersive model. Experimental conditions for (a) and (b) are same as the ones in Fig. 5a and b.

''transport dispersive model'' (Eqs. (2) and (3)) for the same experimental conditions. As seen in Fig. 6a and b, while the transport-dispersive model was successful in predicting the separation at the low salt concentration (50 m*M*), it was unable to capture the improved performance at the higher salt concentration (80 m*M*). Thus, the kinetic-dispersive model was uniquely suited to describe displacement separations in this monolithic system.

5. Conclusions

This paper provides a simple methodology to characterize and simulate preparative ion-exchange chromatography on a monolithic stationary phase. Monolithic stationary phase morphologies were developed in an effort to reduce mass transfer limitations in chromatographic separations. The dimensionless group analysis employed in this paper to compare the relative importance of various non-idealities on chromatographic resins confirms the enhanced mass transfer properties of this morphology. In the absence of significant mass transfer limitations as are observed on conventional beaded morphologies, adsorption/desorption kinetics was found to be the dominant non-ideality on this stationary phase material. This result enabled the selection of an appropriate model for simulating separations on the monolithic stationary phase. Increased buffer salt concentration was shown to result in significant improvements in the performance of displacement separations on this media. While simulations using a mass transfer limited model were unable to effectively simulate these separations, the reactive-dispersive SMA model was well suited for predicting this strong dependence on salt concentration. Thus, this analysis enabled the selection of appropriate operating conditions to improve displacement separation on this media. The results presented in this paper demonstrate the usefulness of this methodology for identifying the dominant non-idealities as well as the importance of selecting the appropriate model for simulating non-linear separations.

6. Nomenclature

b_o	Parameter reflecting retention factor and thereby the salt concentration
C	Mobile phase concentration (m*M*)
C_{salt}	Mobile phase salt concentration (m*M*)
d_p	Particle diameter (cm)
D_a	Axial dispersion coefficient (cm^2/s)
D_m	Molecular diffusivity (cm^2/s)
D_p	Pore diffusion coefficient (cm^2/s)
D'	Effective pore diffusivity (cm^2/s)
D_s	Surface diffusion coefficient (cm^2/s)
F	Flow rate (ml/min)
H	Height equivalent to a theoretical plate (cm)
k'	Retention factor
k_{ads}	Adsorption rate constant ($mM^{-\nu}\ s^{-1}$)
k_{des}	Desorption rate constant ($mM^{-\nu}\ s^{-1}$)
k''_{des}	Parameter defined for Eq. (10) $(=\frac{1-\epsilon_p}{\epsilon_p}K\Lambda^{\gamma}k_{des})$

k_f	Film transport coefficient (cm/s)
k_m	Lumped mass transport coefficient (s^{-1})
K	Equilibrium constant in SMA formalism
L	Length of column (cm)
Pe_a	Peclet number ($=Lu/D_a$)
Q	Stationary phase concentration (mM)
Q	Concentration of bound salt that is not sterically shielded (mM)
Q^{equil}	Equilibrium stationary phase concentration (mM)
r	Ratio of surface diffusion and pore diffusion ($=D_s/D_p$)
R	Particle radius (cm)
St	Stanton number ($=k_mL/u$)
t_r	Retention time (min)
$t_{w,0.5}$	Width at half height (min)
u	Superficial velocity (cm/s)
u'	Intraparticle convective velocity based on the pellet cross sectional area
V_o	Column dead volume (ml)
x	Dimensionless axial distance

Greek

β	Phase ratio ($=(1-\varepsilon_t)/\varepsilon_t$)
Δx	Space grid
$\Delta\tau$	Time grid
ε_i	Interstitial porosity
ε_p	Particle porosity
ε_t	Total porosity
λ_p	Intraparticle Peclet number
ν	Characteristic charge
σ	Steric factor
τ	Dimensionless time
ζ	Axial dispersion parameter (cm) ($=D_a/u$)
Λ	Ionic capacity (mM)

Acknowledgements

The authors would like to acknowledge the National Science Foundation (Grant No. CTS-9416921) for their support of this research and Dr. Bob MacColl and Leslie Eiselle of the Wadsworth Research Center, Albany for the use of some of their equipment.

References

[1] L. Whitney, M. McCoy, N. Gordon, N. Afeyan, Characterization of large-pore polymeric supports for use in perfusion biochromatography, J. Chromatogr. A 807 (1998) 165.
[2] N.B. Afeyan, N.F. Gordon, L. Mazaroff, L. Varady, Y.B. Fulton, J. Regnier, J. Chromatogr. 519 (1990) 1.
[3] B. Boschetti, J.L. Coffman, in: G. Subramanian (Ed.), Bioseparation and Bioprocessing, Wiley-VCH, Weinheim, 1998, p. 157.
[4] P.E. Gustavsson, A. Axelsson, P.O. Larsson, Direct measurements of convective fluid velocities in super porous agarose beds, J. Chromatogr. A 795 (1998) 199.
[5] X. Zeng, E. Ruckenstein, Membrane chromatography: preparation and applications to protein separation, Biotechnol. Prog. 15 (6) (1999) 1003.
[6] S. Hjerten, J.L. Liao, R. Zhang, High-performance liquid chromatography on continuous beds, J. Chromatogr. 473 (1989) 29.
[7] US Pat. 5 645 717; Eur. Pat. EPO407560.
[8] F. Svec, J. Frechet, Continuous rods of macroporous polymer as high-performance liquid chromatography separation media, Anal. Chem. 64 (1992) 820.
[9] D. Sykora, F. Svec, J. Frechet, Separation of oligonucleotides on novel monolithic columns with ion-exchange functional surfaces, J. Chromatogr. A 852 (1999) 297.
[10] H. Minakuchi, N. Ishizuka, K. Nakanishi, N. Soga, N. Tanaka, Performance of an octadecylsilylated continuous porous silica column in polypeptide separations, J. Chromatogr. A 828 (1998) 83.
[11] P.E. Gustavsson, P.O. Larsson, Continuous superporous agarose beds for chromatography and electrophoresis, J. Chromatogr. A 832 (1999) 29.
[12] G. Garke, I. Radtschenko, F.B. Anspach, Continuous-bed chromatography for the analysis and purification of recombinant human basic fibroblast growth factor, J. Chromatogr. A 857 (1999) 137.
[13] R. Giovannini, R. Freitag, High-performance membrane chromatography of supercoiled plasmid DNA, Anal. Chem. 70 (1998) 3348.
[14] S. Vogt, R. Freitag, Displacement chromatography using the UNO continuous bed column as a stationary phase, Biotechnol. Prog. 14 (1998) 742.
[15] S. Vogt, R. Freitag, Separation of plasmid DNA from protein and bacterial lipopolysaccharides using displacement chromatography, Cytotechnology 30 (1999) 159.
[16] R. Freitag, S. Vogt, Comparison of particulate and continuous-bed columns for protein displacement chromatography, J. Biotechnol. 78 (2000) 69.
[17] J.L. Meyers, A.I. Liapis, Network modeling of the convective flow and diffusion of molecules adsorbing in monoliths and in porous particles packed in a chromatographic column, J. Chromatogr. A 852 (1999) 3.
[18] C.A. Brooks, S.M. Cramer, Steric mass-action ion-exchange: displacement profiles and induced salt gradients, AIChE J. 1992 (1969) 38.

[19] S.R. Gallant, A. Kundu, S.M. Cramer, Modeling non-linear elution of proteins in ion-exchange chromatography, J. Chromatogr. A 702 (1995) 125.
[20] S.R. Gallant, S. Vunnum, S.M. Cramer, Optimization of preparative ion-exchange chromatography of proteins: linear gradient separations, J. Chromatogr. A 725 (1999) 295.
[21] A. Shukla, R. Hopfer, D. Chakravarti, E. Bortell, S. Cramer, Purification of an antigenic vaccine protein by selective displacement chromatography, Biotechnol. Prog. 14 (1998) 92.
[22] G. Guiochon, S. Golshan-Shirazi, A. Katti, Fundamentals of Preparative and Nonlinear Chromatography, Academic Press, Boston, 1994.
[23] V. Natarajan, S.M. Cramer, Modeling shock layers in ion-exchange displacement systems, AIChE J. 45 (1) (1999) 27.
[24] V. Natarajan, S.M. Cramer, A methodology for the characterization of ion-exchange resins, Sep. Sci. Technol. 35 (11) (2000) 1719.
[25] S.D. Gadam, G. Jayaraman, S.M. Cramer, Characterization of non-linear adsorption properties of dextran-based polyelectrolyte displacers in ion-exchange systems, J. Chromatogr. 630 (1993) 37.
[26] A. Kundu, A.A. Shukla, K.A. Barnthouse, J. Moore, S.M. Cramer, Displacement chromatography of proteins using sucrose octasulfate, BioPharm. 10 (1997) 64.
[27] R.B. Bird, W.E. Stewart, E.N. Lightfoot, Transport Phenomena, John Wiley & Sons, New York, 1994.
[28] B. Bidlingmaier, K.K. Unger, N. Doehren, Comparative study on the column performance of microparticulate 5-μm C_{18} bonded and monolithic C_{18} bonded reversed-phase columns in high-performance liquid chromatography, J. Chromatogr. A 832 (1999) 11.
[29] A.E. Rodrigues, G. Carta, Diffusion and convection in chromatographic processes using permeable supports with a bidisperse pore structure, Chem. Eng. Sci. 48 (23) (1993) 3927.